

A detection of circumgalactic gas with fast radio bursts

Liam Connor^{1,2,3,*} & Vikram Ravi^{1,2}

¹ Cahill Center for Astronomy and Astrophysics, MC 249-17, California Institute of Technology, Pasadena CA 91125, USA.

² Owens Valley Radio Observatory, California Institute of Technology, Big Pine CA 93513, USA.

³ E-mail: liam.dean.connor@gmail.com

Galaxies and groups of galaxies exist in dark-matter halos filled with diffuse gas. The diffuse gas represents up to 80% of the mass in luminous matter within the halos^{1,2}, and is difficult to detect because of its low density (particle number densities of $\lesssim 10^{-4} \text{ cm}^{-3}$) and high temperature (mostly greater than 10^6 K). The spatial distribution and total mass of this material determines, and is influenced by, the evolution of galaxies and galaxy groups³⁻⁵. Existing observational constraints on these quantities are limited by sensitivity, and the necessity to accurately model the ionization fraction, metal content, and pressure of the gas⁶⁻⁸. Here we report the detection of diffuse gas associated with nearby galaxies using the dispersion measures (DMs) of extragalactic fast radio bursts (FRBs). FRB DMs provide direct measurements of the total ionized-gas contents along their sightlines. Out of a sample of 474 distant FRBs from the CHIME/FRB Catalog 1⁹, we identify a sample of 24 events that likely intersect the dark-matter halos of galaxies in the local Universe ($< 40 \text{ Mpc}$). This subset of FRBs has an excess mean DM of $200 \pm 100 \text{ pc cm}^{-3}$ over those that do not intersect nearby galaxies. The excess is larger than expected for the diffuse gas surrounding isolated galaxies, but may be explained by additional contributions from gas surrounding galaxy groups, including from the Local Group. This result demonstrates the predicted ability of FRBs to be used as sensitive, model-independent measures of the diffuse-gas contents of dark-matter halos¹⁰⁻¹³.

The Canadian Hydrogen Intensity Mapping Experiment (CHIME) Fast Radio Burst Project (CHIME/FRB hereafter) published its first catalog of 535 FRBs detected in the 400–800 MHz radio band between 2018 July 25 and 2019 July 1⁹. CHIME is a transit telescope that observes the whole northern sky daily^{14,15}. The first CHIME/FRB catalog includes one-off bursts from 474 sources,

and 18 repeating sources that are not included in our analysis (Methods). This is the largest collection of FRBs from a single survey by more than an order of magnitude. The uniformity of the sample, both in sky position and in terms of selection effects, provides significant power for statistical inference⁹. For example, a correlation has been observed between the locations of CHIME FRBs and the distribution of known galaxies with cosmological redshifts $0.3 < z < 0.5$, which indicates that the majority of CHIME FRBs originate from correspondingly large distances¹⁶.

Despite its central role in the formation and evolution of galaxies, diffuse gas surrounding galaxies is notoriously difficult to study in detail². We refer to this medium as the circumgalactic medium (CGM) in the case of individual galaxies (dark matter halo masses $10^{11} M_\odot \lesssim M_h \lesssim 10^{13} M_\odot$), the intra-group medium (IGrM) in the case of galaxy groups ($10^{13} M_\odot \lesssim M_h \lesssim 10^{13.5} M_\odot$), and the intracluster medium (ICM) in the case of galaxy clusters ($M_h \gtrsim 10^{13.5} M_\odot$). As short-duration (approximately millisecond) radio-wavelength pulses, FRBs are dispersed during propagation through astrophysical plasmas along their sightlines. The DM to a redshift z is given by the following integral¹⁷:

$$\text{DM}(z) = \frac{c}{H_0} \int_0^z \frac{(1+z)n_e(z)}{\sqrt{(1+z)^3 \Omega_M + \Omega_\Lambda}} dz, \quad (1)$$

where c is the vacuum speed of light, H_0 is the Hubble constant, $n_e(z)$ is the free-electron number density as a function of redshift, Ω_M is the fractional cosmic matter density, and Ω_Λ is the fractional cosmic dark-energy density. The observed DM, DM_{obs} , is conventionally broken down into a series of components:

$$\text{DM}_{\text{obs}} = \text{DM}_{\text{MW}} + \text{DM}_{\text{MWhalo}} + \sum_i^{\text{N}_{\text{gal}}} \text{DM}_{\text{CGM}_i} + \text{DM}_{\text{IGM}} + \text{DM}_{\text{host}}, \quad (2)$$

where DM_{MW} and $\text{DM}_{\text{MWhalo}}$ are contributed by the Milky Way interstellar medium and gaseous

halo respectively, DM_{host} is contributed by the FRB host galaxy, DM_{IGM} is contributed by the intergalactic medium, and the CGM contributions from intervening galaxies (DM_{CGM_i}) are summed over N_{gal} objects. The intergalactic-medium contribution, DM_{IGM} , is often the largest term and is thought to lead to the Macquart (DM– z) relation¹⁹. The exact value of DM_{CGM_i} for a given intervening galaxy will depend on the impact parameter of the background FRB (b_{\perp}), and the unknown spatial gas-density distribution surrounding the galaxy. Individual FRBs have been found to intersect foreground halos^{20,21}, but without the statistics of a larger sample it is difficult to extract the DM contribution of the CGM^{10,11,13}.

CHIME is a compact telescope and lacks the angular resolution to unambiguously identify the host galaxies of FRBs^{22,23}. Typical sky-localization error regions are $\sim 0.2 \times 0.2$ degrees in the CHIME/FRB Catalog 1. We therefore focus this work on nearby, massive galaxies with dark-matter halo virial radii that subtend large angular scales. An approximately Milky-Way sized halo with a virial radius of ~ 200 kpc will be smaller in angular size than a standard CHIME/FRB localization region at distances $\lesssim 40$ Mpc.

We identify a sample of CHIME FRBs that likely intersect nearby halos within a threshold impact parameter (Methods). We have utilized the Gravitational Wave Galaxy Catalogue (GWGC) containing the position, distance, and B -band absolute magnitude (M_B) of 53,255 galaxies within 100 Mpc²⁴. GWGC is likely complete for all galaxies within 40 Mpc with $M_B < -18$; we note that our results are only likely to be diluted by any incompleteness. We begin by using only galaxies with $M_B < -18.5$, that are within 40 Mpc, and are more distant than 500 kpc. For a fiducial threshold impact parameter of $b_{\perp} = 250$ kpc, we find 24 intersecting FRBs. In Figure 1,

we show the sky locations of the full CHIME/FRB catalog of non-repeating FRB sources, as well as the GWGC galaxy / FRB associations within this fiducial b_{\perp} . The list of CHIME/FRB galaxy associations is presented in Extended Data Table 1.

The subset of FRBs that intersect the halos of nearby galaxies have statistically higher extragalactic DMs than the rest of the CHIME/FRB sample. The distributions of DMs in the fiducial sample of CHIME/FRB galaxy intersections, and in the remaining CHIME/FRB sample, are shown in Figure 2. We calculate the extragalactic DM by subtracting a model for the DM_{MW} along each FRB sightline²⁵. In this fiducial sample, we exclude FRBs observed at Galactic latitudes within 5 degrees of the Galactic plane to mitigate systematic errors in the model for DM_{MW} . To determine the significance of the mean-DM excess, we employ a two-sided t-test. For the fiducial b_{\perp} , we find a p-value of 0.033. We also explored the variation in p-value for this test when considering different values of b_{\perp} (Figure 3). For b_{\perp} between approximately 100 kpc and 300 kpc, we find two-sided t-test p-values less than 0.05.

We established the robustness of this result using a series of jackknife tests and variations in our assumptions. Figure 3 shows a jackknife test in which the DMs of CHIME/FRB sources are randomly shuffled for 150 realizations. These re-sampled data are then put through the same cross-matching procedure with $\lesssim 40$ Mpc GWGC galaxies as the real data, and the “intersecting” CHIME/FRB sources are compared with the remaining dataset. The resulting p-value distribution is uniformly distributed between 0 and 1, as expected for random DM samples. The p-values of the true CHIME/FRB galaxy associations rise as a function of impact parameter until there is no statistical difference between the two DM distributions, as expected. The random realizations show no

such trend, nor does any simulated curve have a mean p-value as low as the real data when averaged between 100–300 kpc. As a further test of robustness, we apply different cuts to the CHIME/FRB catalog and GWGC. We alter the M_B cut on foreground galaxies between -17.0 and -19.5 , and vary the maximum galaxy distance between 15 Mpc and 70 Mpc. For the CHIME/FRB sources, we apply various limits on the Galactic latitude (between 0 deg and 20 deg from the Galactic plane), and consider an additional model for DM_{MW} ²⁶ together with no subtraction of DM_{MW} . In all of these cases the excess DM persists with p-values < 0.05 , for $b_{\perp} < 300$ kpc. However, if we consider only GWGC galaxies at distances between 50 Mpc and 100 Mpc the signal disappears, likely because the halos subtend small solid angles relative to the CHIME/FRB localization regions, and the apparent intersections are false. We consider additional means of identifying CHIME/FRB galaxy intersections, and find no change to our results (Methods).

It is unlikely that the FRBs that we associate with nearby galaxy halos in fact originate from these galaxies (Methods). We also find that the total number of intersections is consistent with the expected range for a background population, based on the probability of halo intercepts (Methods). It is also unlikely that these FRBs pass through the disks of the nearby galaxies, both from a statistical perspective, and because the effects of multi-path propagation would render them undetectable²⁷. The excess DM in the CHIME/FRB galaxy intersections can therefore be robustly ascribed to gas in the halos of the nearby galaxies, because there is no other difference in the sample selection.

We next quantify the DM excess as a function of impact parameter. For the fiducial sample of CHIME/FRB galaxy intersections, we find a mean DM of 790 ± 110 pc cm⁻³, and the remainder

of the CHIME/FRB sample has a mean DM of $600 \pm 20 \text{ pc cm}^{-3}$ (1σ errors throughout). As not all the CHIME/FRB galaxy associations are secure, and because positional uncertainty will act to bias the measured DM excess at fixed b_{\perp} downward, it is likely that the true excess is higher. The magnitude and uncertainty for the DM excess is shown for different b_{\perp} in Figure 4. For $b_{\perp} < 350 \text{ kpc}$, the DM excess is $\gtrsim 100 \text{ pc cm}^{-3}$. This does not necessarily mean that the diffuse gas extends to 350 kpc. Each data point is highly correlated between threshold impact parameters, so excess DM at smaller b_{\perp} will appear at larger b_{\perp} as well.

The DM excess ($200 \pm 100 \text{ pc cm}^{-3}$ for our fiducial analysis) is substantially larger than predicted for diffuse gas in the halos of individual galaxies^{10,12}. By estimating the halo masses of the sample of intersected galaxies listed in Extended Data Table 1, we find predicted DM excesses less than 40 pc cm^{-3} even in the case that these halos retain the expected cosmic fraction of baryons (see Methods and Extended Data Figure 1). However, over two thirds of the FRB/galaxy intersections are with galaxies that belong to groups (Extended Data Table 1); this is not unexpected²⁸. Intersected groups include the Local Group, the M81 Group, and the M74 Group. Galaxy groups host a rich IGrM, aspects of which have been extensively studied through extended thermal X-ray emission²⁹, ultraviolet absorption spectroscopy³⁰, and its impact on the cosmic microwave background (the Sunyaev-Zel'dovich / SZ effect)³¹. It is likely that galaxy groups retain significant fractions of their expected baryon contents in a hot ($> 10^6 \text{ K}$) phase, although the effects of energy feedback may complicate the exact distributions of temperature and density⁵. The observed DM excess is nonetheless consistent with simple models for the DM contribution from the IGrM (Methods)^{12,32}.

If we consider only the CHIME FRBs that intersect the halos of Local Group galaxies M31 and M33, we still see a considerable excess DM. We note that the DM excess persists in the remaining intersected-galaxy sample, excluding the Local Group. If the Local Group IGrM is modeled with a dark matter halo mass of $10^{12.5} M_{\odot}$, it likely contributes a DM of $> 100 \text{ pc cm}^{-3}$ over tens of degrees on the sky in the direction of M31¹². Our data are also consistent with recent analyses of X-ray O VII and O VIII emission lines and SZ maps that indicate significant hot-gas content extended to an angular radius of approximately 30 degrees from M31³³. This is suggested to represent a hot-gas bridge connecting the Milky Way with M31 and M33 that corresponds to a DM of 80–400 pc cm^{-3} . We anticipate that our measurements, when augmented by additional data from CHIME/FRB and other instruments, will significantly aid in the modeling and interpretation of the X-ray and SZ observations of the Local Group IGrM, together with the IGrM of other nearby intersected groups.

The magnitude of the observed DM excess in the CHIME/FRB galaxy intersections is promising for future FRB-DM measurements of the mass and density profile of diffuse gas surrounding galaxies and galaxy groups. For example, with a larger FRB sample, the analysis presented here can be applied to galaxy clusters, where the $10^{14-15} M_{\odot}$ halos with virial radii of around 2 Mpc may contribute DMs greater than 10^3 pc cm^{-3} ^{12,32}. We note that the most highly dispersed CHIME/FRB source, with extragalactic DM = $3006.7 \text{ pc cm}^{-3}$, appears to intersect within 1.4 Mpc of the center of the galaxy cluster J185.83917+56.47005 at $z=0.328$, found by cross-matching with the GMBCG cluster catalog³⁴.

References

1. Anderson, M. E. & Bregman, J. N. Do Hot Halos Around Galaxies Contain the Missing Baryons? *The Astrophysical Journal* **714**, 320–331, DOI: <https://dx.doi.org/10.1088/0004-637X/714/1/320> (2010). 1003.3273.
2. Tumlinson, J., Peebles, M. S. & Werk, J. K. The Circumgalactic Medium. *Annual Review of Astron and Astrophys* **55**, 389–432, DOI: <https://dx.doi.org/10.1146/annurev-astro-091916-055240> (2017). 1709.09180.
3. Fukugita, M. & Peebles, P. J. E. The Cosmic Energy Inventory. *The Astrophysical Journal* **616**, 643–668, DOI: <https://dx.doi.org/10.1086/425155> (2004). astro-ph/0406095.
4. Fielding, D., Quataert, E., McCourt, M. & Thompson, T. A. The impact of star formation feedback on the circumgalactic medium. *Monthly Notices of the Royal Astronomical Society* **466**, 3810–3826, DOI: <https://dx.doi.org/10.1093/mnras/stw3326> (2017). 1606.06734.
5. Oppenheimer, B. D., Babul, A., Bahé, Y., Butsky, I. S. & McCarthy, I. G. Simulating Groups and the IntraGroup Medium: The Surprisingly Complex and Rich Middle Ground between Clusters and Galaxies. *Universe* **7**, 209, DOI: <https://dx.doi.org/10.3390/universe7070209> (2021). 2106.13257.
6. Werk, J. K. *et al.* The COS-Halos Survey: Physical Conditions and Baryonic Mass in the Low-redshift Circumgalactic Medium. *The Astrophysical Journal* **792**, 8, DOI: <https://dx.doi.org/10.1088/0004-637X/792/1/8> (2014). 1403.0947.
7. Bregman, J. N. *et al.* The Extended Distribution of Baryons around Galaxies. *The Astrophysical Journal* **862**, 3, DOI: <https://dx.doi.org/10.3847/1538-4357/aacafe> (2018). 1803.08963.

8. Lim, S. H., Mo, H. J., Wang, H. & Yang, X. Detection of Missing Baryons in Galaxy Groups with Kinetic Sunyaev-Zel'dovich Effect. *The Astrophysical Journal* **889**, 48, DOI: <https://dx.doi.org/10.3847/1538-4357/ab63df> (2020). 1912.10152.
9. The CHIME/FRB Collaboration *et al.* The First CHIME/FRB Fast Radio Burst Catalog. *arXiv e-prints* arXiv:2106.04352 (2021). 2106.04352.
10. McQuinn, M. Locating the “Missing” Baryons with Extragalactic Dispersion Measure Estimates. *The Astrophysical Journal Letters* **780**, L33 (2014).
11. Ravi, V. Measuring the Circumgalactic and Intergalactic Baryon Contents with Fast Radio Bursts. *The Astrophysical Journal* **872**, 88, DOI: <https://dx.doi.org/10.3847/1538-4357/aafb30> (2019). 1804.07291.
12. Prochaska, J. X. & Zheng, Y. Probing Galactic haloes with fast radio bursts. *Monthly Notices of the Royal Astronomical Society* **485**, 648–665, DOI: <https://dx.doi.org/10.1093/mnras/stz261> (2019). 1901.11051.
13. Madhavacheril, M. S., Battaglia, N., Smith, K. M. & Sievers, J. L. Cosmology with the kinematic Sunyaev-Zeldovich effect: Breaking the optical depth degeneracy with fast radio bursts. *Physical Review D* **100**, 103532, DOI: <https://dx.doi.org/10.1103/PhysRevD.100.103532> (2019).
14. Bandura, K. *et al.* Canadian Hydrogen Intensity Mapping Experiment (CHIME) pathfinder. In Stepp, L. M., Gilmozzi, R. & Hall, H. J. (eds.) *Ground-based and Airborne Telescopes V*, vol. 9145 of *Society of Photo-Optical Instrumentation Engineers (SPIE) Conference Series*, 914522, DOI: <https://dx.doi.org/10.1117/12.2054950> (2014). 1406.2288.

15. Kaspi, V. M. & CHIME/FRB Collaboration. The CHIME Fast Radio Burst Project. In *American Astronomical Society Meeting Abstracts #229*, vol. 229 of *American Astronomical Society Meeting Abstracts*, 242.19 (2017).
16. Rafiei-Ravandi, M. *et al.* CHIME/FRB Catalog 1 results: statistical cross-correlations with large-scale structure. *arXiv e-prints* arXiv:2106.04354 (2021). [2106.04354](https://arxiv.org/abs/2106.04354).
17. Shull, J. M. & Danforth, C. W. The Dispersion of Fast Radio Bursts from a Structured Intergalactic Medium at Redshifts $z < 1.5$. *The Astrophysical Journal Letters* **852**, L11, DOI: <https://dx.doi.org/10.3847/2041-8213/aaa2fa> (2018). [1712.01280](https://arxiv.org/abs/1712.01280).
18. Macquart, J. P. & Ekers, R. FRB event rate counts - II. Fluence, redshift, and dispersion measure distributions. *Monthly Notices of the Royal Astronomical Society* **480**, 4211–4230, DOI: <https://dx.doi.org/10.1093/mnras/sty2083> (2018). [1808.00908](https://arxiv.org/abs/1808.00908).
19. Macquart, J. P. *et al.* A census of baryons in the Universe from localized fast radio bursts. *Nature* **581**, 391–395, DOI: <https://dx.doi.org/10.1038/s41586-020-2300-2> (2020). [2005.13161](https://arxiv.org/abs/2005.13161).
20. Prochaska, J. X. *et al.* The low density and magnetization of a massive galaxy halo exposed by a fast radio burst. *Science* **365**, aay0073, DOI: <https://dx.doi.org/10.1126/science.aay0073> (2019). [1909.11681](https://arxiv.org/abs/1909.11681).
21. Connor, L. *et al.* A bright, high rotation-measure FRB that skewers the M33 halo. *Monthly Notices of the Royal Astronomical Society* **499**, 4716–4724, DOI: <https://dx.doi.org/10.1093/mnras/staa3009> (2020). [2002.01399](https://arxiv.org/abs/2002.01399).

22. Eftekhari, T. & Berger, E. Associating Fast Radio Bursts with Their Host Galaxies. *The Astrophysical Journal* **849**, 162, DOI: <https://dx.doi.org/10.3847/1538-4357/aa90b9> (2017). 1705.02998.
23. Aggarwal, K. *et al.* Probabilistic Association of Transients to their Hosts (PATH). *The Astrophysical Journal* **911**, 95, DOI: <https://dx.doi.org/10.3847/1538-4357/abe8d2> (2021). 2102.10627.
24. White, D. J., Daw, E. J. & Dhillon, V. S. A list of galaxies for gravitational wave searches. *Classical and Quantum Gravity* **28**, 085016, DOI: <https://dx.doi.org/10.1088/0264-9381/28/8/085016> (2011).
25. Cordes, J. M. NE2001: A New Model for the Galactic Electron Density and its Fluctuations. In Clemens, D., Shah, R. & Brainerd, T. (eds.) *Milky Way Surveys: The Structure and Evolution of our Galaxy*, vol. 317 of *Astronomical Society of the Pacific Conference Series*, 211 (2004).
26. Yao, J. M., Manchester, R. N. & Wang, N. A New Electron-density Model for Estimation of Pulsar and FRB Distances. *The Astrophysical Journal* **835**, 29, DOI: <https://dx.doi.org/10.3847/1538-4357/835/1/29> (2017). 1610.09448.
27. Prochaska, J. X. & Neeleman, M. The astrophysical consequences of intervening galaxy gas on fast radio bursts. *Monthly Notices of the Royal Astronomical Society* **474**, 318–325, DOI: <https://dx.doi.org/10.1093/mnras/stx2824> (2018). 1711.00323.
28. Yang, X. *et al.* Galaxy Groups in the SDSS DR4. I. The Catalog and Basic Properties. *The Astrophysical Journal* **671**, 153–170, DOI: <https://dx.doi.org/10.1086/522027> (2007). 0707.4640.

29. Mulchaey, J. S. X-ray Properties of Groups of Galaxies. *Annual Review of Astronomy and Astrophysics* **38**, 289–335, DOI: <https://dx.doi.org/10.1146/annurev.astro.38.1.289> (2000). [astro-ph/0009379](https://arxiv.org/abs/astro-ph/0009379).
30. Stocke, J. T. *et al.* Absorption-line Detections of 10^5 - 10^6 K Gas in Spiral-rich Groups of Galaxies. *The Astrophysical Journal* **791**, 128, DOI: <https://dx.doi.org/10.1088/0004-637X/791/2/128> (2014). [1405.4307](https://arxiv.org/abs/1405.4307).
31. Planck Collaboration *et al.* Planck 2013 results. XVI. Cosmological parameters. *Astronomy and Astrophysics* **571**, A16, DOI: <https://dx.doi.org/10.1051/0004-6361/201321591> (2014). [1303.5076](https://arxiv.org/abs/1303.5076).
32. Fujita, Y., Akahori, T., Umetsu, K., Sarazin, C. L. & Wong, K.-W. Probing WHIM around Galaxy Clusters with Fast Radio Bursts and the Sunyaev-Zel'dovich effect. *The Astrophysical Journal* **834**, 13, DOI: <https://dx.doi.org/10.3847/1538-4357/834/1/13> (2017). [1609.03566](https://arxiv.org/abs/1609.03566).
33. Qu, Z., Huang, R., Bregman, J. N. & Li, J.-T. An X-Ray- and SZ-bright Diffuse Source toward M31: A Local Hot Bridge. *The Astrophysical Journal* **907**, 14, DOI: <https://dx.doi.org/10.3847/1538-4357/abc9b9> (2021). [2011.02125](https://arxiv.org/abs/2011.02125).
34. Hao, J. *et al.* VizieR Online Data Catalog: GMBCG galaxy cluster catalog from SDSS DR7 (Hao+, 2010). *VizieR Online Data Catalog J/ApJS/191/254* (2013).
35. Lu, W. & Piro, A. L. Implications from ASKAP Fast Radio Burst Statistics. *The Astrophysical Journal* **883**, 40, DOI: <https://dx.doi.org/10.3847/1538-4357/ab3796> (2019). [1903.00014](https://arxiv.org/abs/1903.00014).

36. Gardenier, D. W., Connor, L., van Leeuwen, J., Oostrum, L. C. & Petroff, E. Synthesising the repeating FRB population using frbpoppy. *Astronomy and Astrophysics* **647**, A30, DOI: <https://dx.doi.org/10.1051/0004-6361/202039626> (2021). 2012.02460.
37. Shull, J. M., Smith, B. D. & Danforth, C. W. The Baryon Census in a Multiphase Intergalactic Medium: 30% of the Baryons May Still be Missing. *The Astrophysical Journal* **759**, 23, DOI: <https://dx.doi.org/10.1088/0004-637X/759/1/23> (2012). 1112.2706.
38. Planck Collaboration *et al.* Planck 2018 results. VI. Cosmological parameters. *Astronomy and Astrophysics* **641**, A6, DOI: <https://dx.doi.org/10.1051/0004-6361/201833910> (2020). 1807.06209.
39. Shull, J. M. Where do Galaxies End? *The Astrophysical Journal* **784**, 142, DOI: <https://dx.doi.org/10.1088/0004-637X/784/2/142> (2014). 1401.5799.
40. Jones, C. & Forman, W. The structure of clusters of galaxies observed with Einstein. *The Astrophysical Journal* **276**, 38–55, DOI: <https://dx.doi.org/10.1086/161591> (1984).
41. Miller, M. J. & Bregman, J. N. Constraining the Milky Way’s Hot Gas Halo with O VII and O VIII Emission Lines. *The Astrophysical Journal* **800**, 14, DOI: <https://dx.doi.org/10.1088/0004-637X/800/1/14> (2015). 1412.3116.
42. Watkins, L. L., van der Marel, R. P., Sohn, S. T. & Evans, N. W. Evidence for an Intermediate-mass Milky Way from Gaia DR2 Halo Globular Cluster Motions. *The Astrophysical Journal* **873**, 118, DOI: <https://dx.doi.org/10.3847/1538-4357/ab089f> (2019). 1804.11348.

43. Karachentsev, I. D., Karachentseva, V. E., Huchtmeier, W. K. & Makarov, D. I. A Catalog of Neighboring Galaxies. *The Astronomical Journal* **127**, 2031–2068, DOI: <https://dx.doi.org/10.1086/382905> (2004).
44. Shannon, R. M. *et al.* The dispersion-brightness relation for fast radio bursts from a wide-field survey. *Nature* **562**, 386–390, DOI: <https://dx.doi.org/10.1038/s41586-018-0588-y> (2018).
45. James, C. W. *et al.* The fast radio burst population evolves, consistent with the star-formation rate. *arXiv e-prints* arXiv:2101.07998 (2021). [2101.07998](https://arxiv.org/abs/2101.07998).
46. James, C. W. *et al.* The z -DM distribution of fast radio bursts. *arXiv e-prints* arXiv:2101.08005 (2021). [2101.08005](https://arxiv.org/abs/2101.08005).
47. Niu, C.-H. *et al.* CRAFTS for Fast Radio Bursts: Extending the Dispersion-Fluence Relation with New FRBs Detected by FAST. *The Astrophysical Journal Letters* **909**, L8, DOI: <https://dx.doi.org/10.3847/2041-8213/abe7f0> (2021). [2102.10546](https://arxiv.org/abs/2102.10546).
48. Heintz, K. E. *et al.* Host Galaxy Properties and Offset Distributions of Fast Radio Bursts: Implications for Their Progenitors. *The Astrophysical Journal* **903**, 152, DOI: <https://dx.doi.org/10.3847/1538-4357/abb6fb> (2020). [2009.10747](https://arxiv.org/abs/2009.10747).
49. Connor, L. Interpreting the distributions of FRB observables. *Monthly Notices of the Royal Astronomical Society* **487**, 5753–5763, DOI: <https://dx.doi.org/10.1093/mnras/stz1666> (2019). [1905.00755](https://arxiv.org/abs/1905.00755).
50. Simard, D. & Ravi, V. Measuring interstellar turbulence in fast radio burst host galaxies. *arXiv e-prints* arXiv:2107.11334 (2021). [2107.11334](https://arxiv.org/abs/2107.11334).

51. Lu, W. & Piro, A. L. Implications from ASKAP Fast Radio Burst Statistics. *The Astrophysical Journal* **883**, 40, DOI: <https://dx.doi.org/10.3847/1538-4357/ab3796> (2019). 1903.00014.
52. Zhang, R. C., Zhang, B., Li, Y. & Lorimer, D. R. On the energy and redshift distributions of fast radio bursts. *Monthly Notices of the Royal Astronomical Society* **501**, 157–167, DOI: <https://dx.doi.org/10.1093/mnras/staa3537> (2021). 2011.06151.

Supplementary Information is linked to the online version of the paper at www.nature.com/nature.

Acknowledgements. We thank Cameron Hummels, Wenbin Lu, J. Michael Shull, and the Caltech FRB group for a helpful discussions. This research was partially supported by the National Science Foundation under grant AST-1836018.

Author contributions. V.R. conceived of searching only nearby foreground galaxies for FRB/halo interceptions. L.C. developed the methods for cross-matching the catalogs, statistically testing the DM distributions, and analyzing the DM excess that are reported in the main text figures and results. V.R. modeled the halo DM contribution shown in Extended Data Figures 1 and 2. L.C led the writing of the manuscript in close collaboration with V.R.

Author information. Correspondence and requests for materials should be addressed to Dr. Liam Connor at liam.dean.connor@gmail.com.

Competing interests statement. The authors declare that they have no competing financial interests.

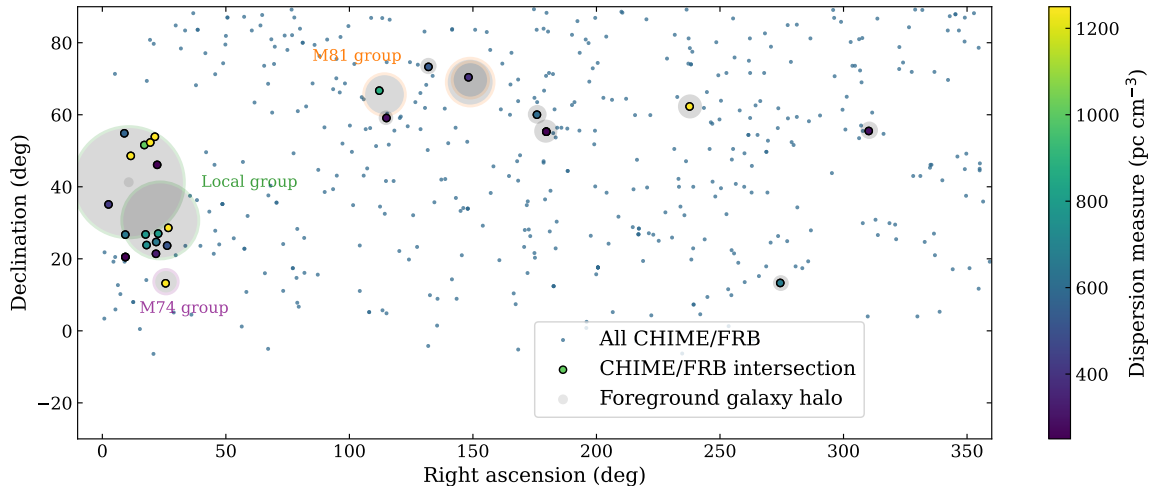


Figure 1 CHIME/FRB galaxy intersections. We show the sky locations of 474 one-off FRB sources in the CHIME/FRB Catalog 1⁹, with those that intersect nearby (< 40 Mpc) GWGC galaxies (grey circles) using the fiducial $b_{\perp} = 250$ kpc indicated by larger dots. The color of the intersecting FRBs encodes their individual extragalactic DMs (as indicated in the color bar), and the remainder of the CHIME/FRB sources are colored by the mean DM value of the non-intersecting sample. Although the color bar is saturated at 1250 pc cm^{-3} , some FRBs that intersect foreground galaxy halos have significantly higher DMs (Extended Data Table 1). The radii of the filled grey circles correspond to the angular size using the galaxy’s estimated virial radius at that distance. Specific galaxy groups are indicated by colored circles around the galaxy locations.

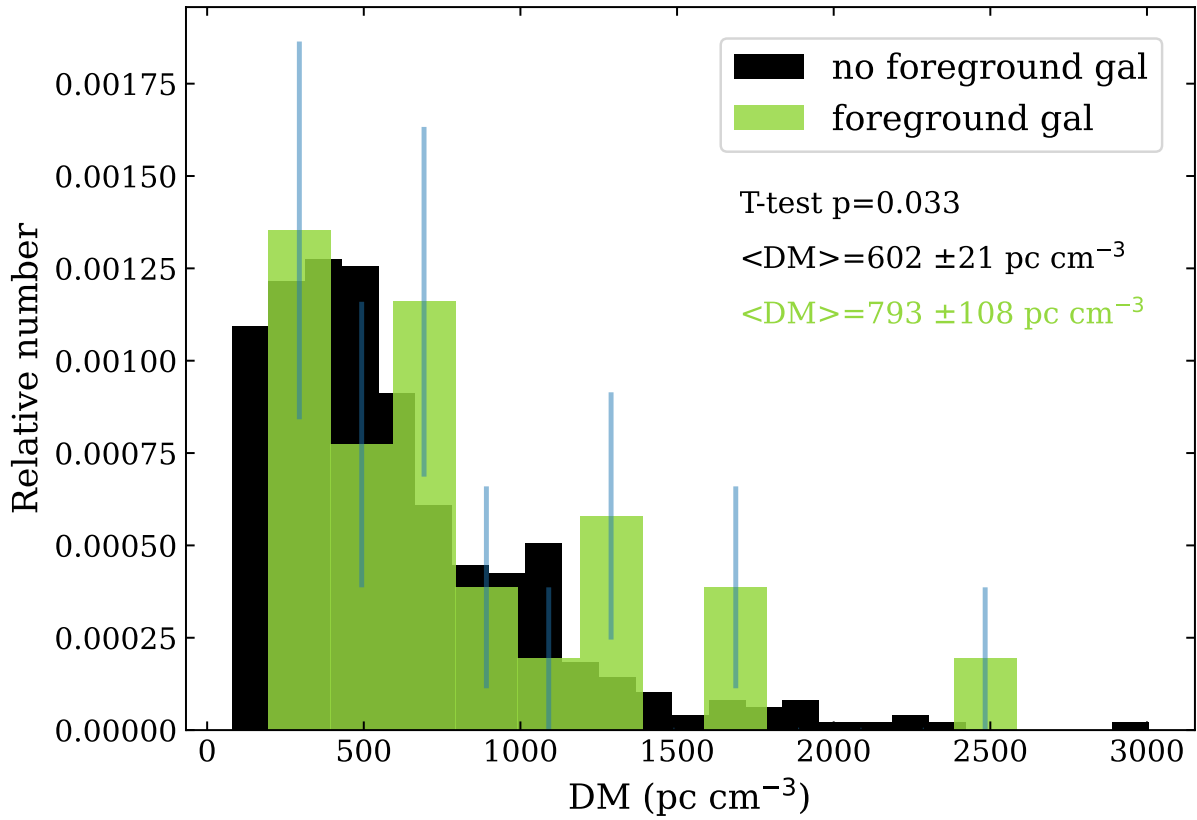


Figure 2 The normalized DM distributions of CHIME FRBs that intersect foreground galaxies (green) and those that do not (black). Here we have used a fiducial value for the threshold impact parameter of $b_{\perp} = 250$ kpc. The 1σ error bars (blue lines) for the CHIME/FRB galaxy intersections are calculated assuming Poisson statistics. The mean DMs of each sample are noted in the figure, together with their 1σ uncertainties.

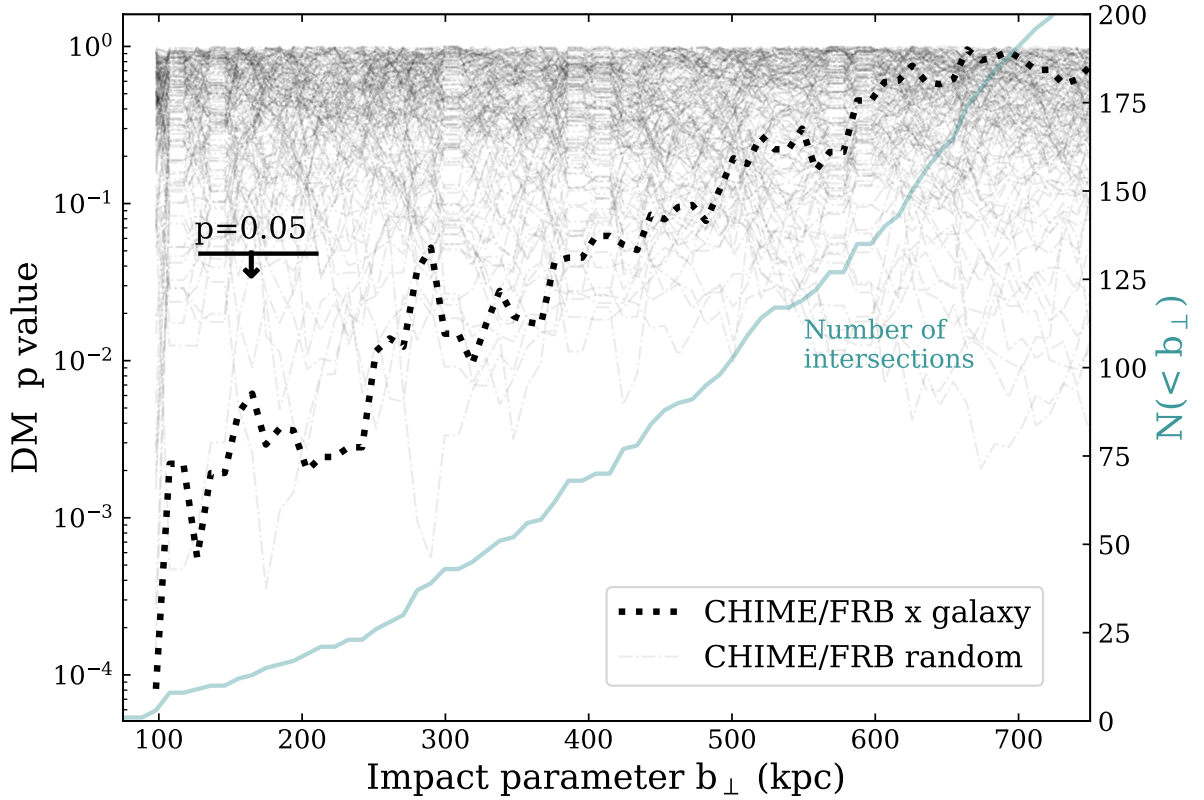


Figure 3 Statistical significance of the excess DM. The primary vertical axis (left) shows the p-value as a function of threshold impact parameter b_{\perp} when computing two-sample t-tests between the DMs of FRBs that intersect foreground halos with those FRBs that do not (thick dotted curve). A jackknife test with a random shuffling of DMs among the CHIME/FRB sources (thin dot dashed curves) is also shown for 150 realizations. None of these simulations exhibit the rising trend in p-value with b_{\perp} that is evident in the real data. The number of CHIME/FRB sources that pass a foreground galaxy for different choices of b_{\perp} is plotted as a cyan solid curve (right vertical axis).

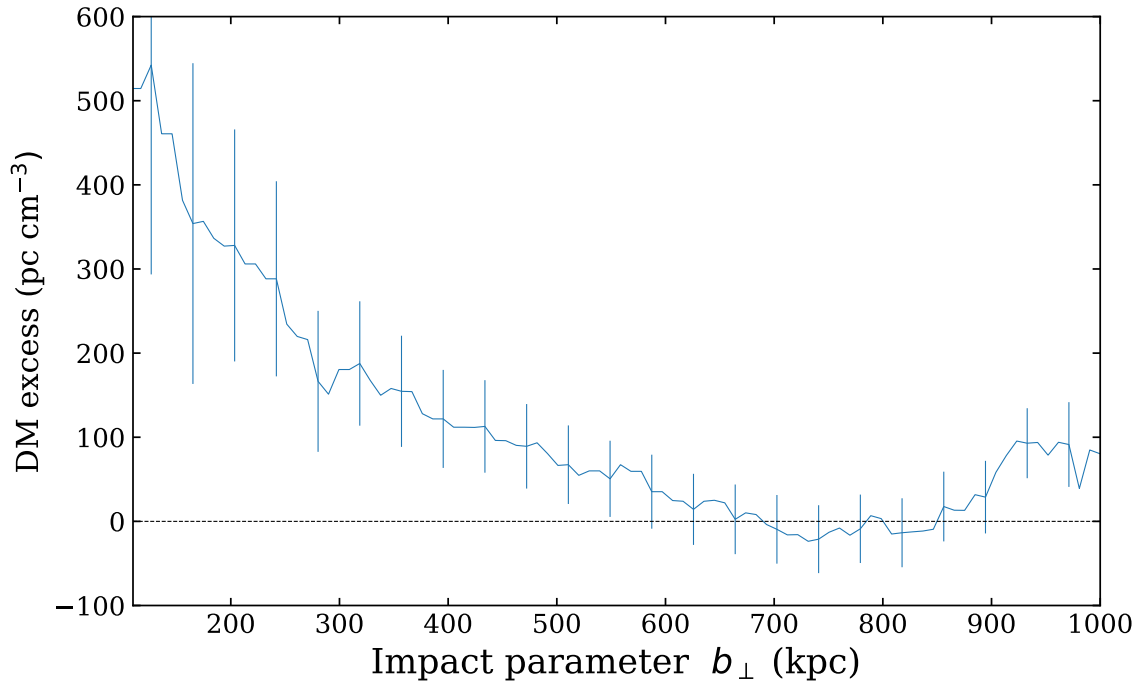


Figure 4 The DM excess for CHIME/FRB galaxy intersections for different choices of b_{\perp} .

1σ error bars are indicated. The data points are highly correlated in threshold impact parameter because they correspond to overlapping sets of CHIME/FRB sources, and so we caution against interpreting the spatial extent of the DM excess in this plot without detailed modeling.

Methods

Sample selection. We used the 474 non-repeating CHIME/FRB sources published in Catalog 1⁹. We exclude the 18 repeating sources in case they have different distance or DM distributions than apparent non-repeaters. This could arise from the bias towards seeing two or more bursts from nearby objects^{35,36}, or if repeaters have preferentially larger DM_{host} . The CHIME/FRB Catalog 1 has three different DM fields: ‘dm_fitb’ is the best fit total DM of the observed FRB. ‘dm_exc_ne2001’, and ‘dm_exc_ymw16’ correspond to total DM minus the expected Milky Way contribution in that direction from the NE2001²⁵ and YMW16²⁶ models respectively. We are concerned here with extragalactic DM, so we opt to use ‘dm_exc_ne2001’. However, all three fields produce similar results in our analysis. To avoid potential uncertainties in modeling the Galactic interstellar medium, we exclude CHIME/FRB sources with an absolute value of Galactic latitude less than 5 degrees, and consider a range of limits between 0 and 20 degrees.

The Gravitational Wave Galaxy Catalogue (GWGC) contains sky position, distance, B -band magnitude, and galaxy type for 53,255 galaxies within 100 Mpc²⁴. We select only galaxies at distances less than 40 Mpc such that their angular size is large enough to associate with the CHIME/FRB uncertainty region. We also set a minimum distance of 0.5 Mpc so as to exclude globular clusters and the Magellanic Clouds. Finally, we use only galaxies whose absolute B -band magnitude is less than -18.5 , and explore limits between -17.0 and -19.5 . The fiducial cut leaves 2829 galaxies. This corresponds to a density of roughly 0.01 Mpc^{-3} . The optical depth of galaxies with an average virial radius R_{vir} out to a maximum distance d_{max} is then $\tau \approx 0.01 \text{ Mpc}^{-3} \cdot d_{\text{max}} \cdot \pi R_{\text{vir}}^2 \approx 0.05$ if we assume the mean virial radius is 200 kpc. We

therefore expect approximately 20–25 CHIME/FRB \times galaxy intersections. This is in line with our observations (teal solid curve in Figure 3).

We have cross-matched the CHIME/FRB Catalog 1 with a subset of the GWGC to look for FRBs for which,

$$R_{\perp}(\theta_{ML}) \lesssim R_{vir} \quad (3)$$

which we parameterize as,

$$R_{\perp}(\theta_{ML}) \leq b_{\perp} \times \left(\frac{M_h}{1.3 \times 10^{12} M_{\odot}} \right)^{1/3}. \quad (4)$$

Here, R_{\perp} is the impact parameter of the CHIME/FRB source at the reported maximum likelihood position, θ_{ML} . M_h is the dark matter halo mass estimated from the galaxy’s absolute B -band magnitude and b_{\perp} is the impact parameter threshold for a galaxy with a Milky Way halo mass. We allow b_{\perp} to vary for Figure 3, but fix it at 250 kpc for Figures 1 and 2. We have tried two other methods for associating CHIME FRBs with galaxies. The first is to ignore galaxy mass and assume a halo was intersected if $R_{\perp}(\theta_{ML}) \leq b_{\perp}$. The second was to use the CHIME/FRB localization confidence interval arrays, provided with their data release¹. Using these arrays, we take a confidence-weighted average of the impact parameter as opposed to using a single maximum-likelihood position. If this weighted mean $\langle R_{\perp}(\theta_{ML}) \rangle$ is less than some value, it is considered an interception. In all three cross-matching methods, we find similar results for the statistical significance of the difference in mean DMs, as well as similar amplitudes for the DM excess.

Jackknife tests and catalog cuts. The p-value of our two-sample t-test can be interpreted as the probability that the two DM distributions (galaxy-intersecting and non-intersecting CHIME/FRB

¹<https://chime-frb-open-data.github.io/localization.html>

sources) have consistent mean values. For threshold impact parameter $b_{\perp} \lesssim 300$ kpc, we find statistically significant differences in mean DM (dotted black curve, Figure 3) using this test. Another method of estimating how unusual our observed DM excess is comes from re-sampling the data. One such jackknife test can be done by randomly shuffling the dispersion measures of CHIME/FRB sources, while keeping their positions unaltered. The p-values for the two shuffled subsets can be computed as a function of b_{\perp} in the same way as the unshuffled data, resulting in the 150 lighter dashed curves in Figure 3. We can then ask, in what fraction of re-samplings do we find an excess equal to or greater than what is observed. We find that in fewer than 1% of re-samplings are the p-values below $b_{\perp} \approx 300$ kpc as small as the real data.

Another scenario where we expect the DM excess signal to disappear is when the foreground galaxies are too far away for the CHIME/FRB localization region to be unambiguously matched with the galaxy’s halo. While there will be many “intersections” due to the increasing optical depth with distance, most will be false positives because the CHIME/FRB localization uncertainty becomes significantly larger than the halo for distances beyond 40 Mpc. We therefore do not expect excess DM if the minimum galaxy distance is set to $\gtrsim 40$ Mpc in the GWGC catalog. And indeed, we find only p-values greater than 0.05 with this cut, despite dozens of reported intersections at $100 \text{ kpc} \leq b_{\perp} \leq 300 \text{ kpc}$.

Interpretation: gas in galaxy halos. Our understanding of the warm/hot gaseous contents of dark matter halos hosting galaxies, galaxy groups and galaxy clusters remains foggy. However, it has long been known that this medium is of significant astrophysical importance, because it represents between 80–90% of the baryon contents of dark matter halos^{1,2,37}. Fundamental open ques-

tions include the total mass and radial density profile of the CGM/IGrM/ICM; FRB observations are a promising new technique to address these questions¹⁰⁻¹³. We express the CGM/IGrM/ICM mass as a fraction, f_{gas} , of the expected baryonic mass in a given dark-matter halo, $\Omega_b M_h / \Omega_M$, where $\Omega_b = 0.049$ is the fractional cosmic baryon density and $\Omega_M = 0.315$ is the fractional cosmic matter density³⁸.

Existing observational probes of f_{gas} for individual galaxies and galaxy groups are beset by systematic issues, and yield uncertain results in comparison with galaxy cluster measurements. The thermal X-ray emission and thermal/kinetic Sunyaev-Zel'dovich (SZ) measurements that are used for galaxy clusters become less reliable for lower halo masses because of decreasing emission columns, lower gas pressures, and the increased effects of feedback from astrophysical processes in galaxies. Individual galaxy halos at low redshifts retain a multi-phase CGM, with a high covering fraction of cool ($\sim 10^4 - 10^5$ K; and therefore primarily ionized) clouds interspersed within the hot ($\gtrsim 10^6$ K), diffuse gas probed by X-ray and SZ observations^{2,7}. Intriguingly, stacked SZ observations of galaxies and galaxy clusters are beginning to reveal a potentially self-similar relation between the inferred signal and M_h , indicating both a universal f_{gas} close to unity and radial density profile^{8,31}. This is consistent with extrapolations of X-ray observations of the IGrM²⁹, but potentially in tension with X-ray observations of individual galaxies⁷. The tension may be resolved by considering feedback effects in different samples, and the existence of significant gas fractions at sub-virial temperatures. Significant other uncertainties remain, including the mass fractions of cool gas in galaxy halos², and indeed the true extents of galaxies³⁹.

In the following, we consider the expected DM excess for our sample of FRB sightlines that

intercept nearby galaxy halos. We first consider each galaxy in isolation, and derive the expected DM accrued for each intercept under two models for the radial number-density distribution of baryons in halos, $n(r)$:

- The fiducial modified Navarro-Frenk-White (mNFW) profile described in¹².
- A ‘beta’ model^{40,41}

$$n(r) = n_0 \left(1 + \left(\frac{r}{r_c} \right)^2 \right)^{-3\beta/2}, \quad (5)$$

where n_0 is a normalization constant, r_c is a core radius that we fix to 1% of the virial radius, and β is an index that we set to 0.5 for consistency with observations of galaxy and galaxy-cluster halos⁷.

In all cases, we fix $f_{\text{gas}} = 1$, and approximately derive the halo masses by scaling the approximate Milky Way halo mass⁴² of $1.3 \times 10^{12} M_{\odot}$ by the ratio between the absolute B -band magnitudes of the GWGC galaxies and the Milky Way B -band magnitude of -20.8 ⁴³. We account for the primordial helium fraction in deriving the DM for each intercept.

The distribution of expected DM excesses for the fiducial sample of 24 FRB / nearby-galaxy intercepts for $b_{\perp} < 250$ kpc is shown in Extended Data Figure 1. We find mean excess DMs for the mNFW and beta models of 34.7 pc cm^{-3} and 38.7 pc cm^{-3} respectively, well below the measured value of $200 \pm 100 \text{ pc cm}^{-3}$. This analysis also demonstrates how the distribution of excesses is sensitive to the chosen radial density profile. More centrally concentrated profiles like the mNFW model result in distributions with longer tails. Consistent with previous works that derive the expected DM excesses for typical galaxy-halo intercepts^{11,12}, we conclude that gas

within individual galaxy halos is insufficient to explain the observed excess in the FRB / nearby-galaxy sample. Although this analysis is approximate by factors of a few due to uncertainties in the halo mass determination, this conclusions are robust because of our conservative assumption of $f_{\text{gas}} = 1$, and because the uncertainty in the CHIME/FRB source positions will only tend to bias the adopted impact parameters towards larger values compared with the true impact parameters.

To illustrate how this problem may be solved, we next consider the expected excess DM accrued by FRBs intersecting halos of different masses. Using the same models for $n(r)$ as above, we simulate 100 samples of 24 random intercepts with $b_{\perp} < 250$ kpc for local ($z = 0$) halos of different masses. We assume a uniform spatial distribution of FRBs. The resulting mean DM excesses for halo masses $10^{12} M_{\odot} \leq M_h \leq 10^{13.5} M_{\odot}$ are shown in Extended Data Figure 2. Consistency between the simulated and measure DM excesses is only achieved for $M_h \gtrsim 10^{12.75} M_{\odot}$, which is approximately four times larger than the Milky Way halo mass. Again, consistent with previous results¹², this analysis makes it clear that membership of the intercepted galaxies in even modest galaxy groups can explain the observed DM excess.

Interpretation: excess host DM. In this section, we consider and reject the possibility that the effect that we observe is explained by a high DM local to FRB host galaxies (DM_{host}). The argument is as follows. First, assume that the FRBs that appear to be spatially coincident with nearby galaxy halos in fact originate from within the nearby galaxies. Now, assuming no cosmic evolution in the typical DM_{host} , nearby FRBs will have typically larger values of DM_{host} than more distant FRBs, because of the suppression of the local DM contribution by a factor $(1 + z)^{-1}$. If all CHIME FRBs are observed at sufficiently low redshifts such that DM_{host} is the dominant

contributor to the total extragalactic DM, then it is possible that the extragalactic DMs of FRBs in fact reduce with increasing redshift. In this contrived example, sources that are close to nearby galaxies on sky will have higher observed DM than those that are not.

This scenario is not supported by any observations in hand. The extragalactic DMs of FRBs with host-galaxy redshift measurements typically increase with increasing redshift, and are dominated by gas external to galaxies¹⁹. The distributions of fluence and DM for FRBs observed at the Parkes, ASKAP, FAST and CHIME telescopes are consistent with a population that exhibits a positive correlation between distance and DM^{9,44–47}. All FRBs localized to host galaxies have $DM_{\text{host}} \lesssim 300 \text{ pc cm}^{-348}$. It is additionally possible that FRBs with high values of DM_{host} will also undergo excess temporal broadening due to interstellar scattering in their host galaxies, which would make them harder to detect^{49,50}.

We nonetheless proceed with a simulation to demonstrate what values of DM_{host} and redshift upper-bounds on the CHIME population (z_{max}) are required to explain the DM excess we observe in the FRB / nearby-galaxy associations. Specifically, under different models, we compare the mean DM for FRBs at distances less than 40 Mpc with the mean DM of FRBs at redshifts $z < z_{\text{max}}$. This simulation has the following components.

- We first need to establish an FRB luminosity function, dN/dL , where N is the comoving number density of FRBs, and L is the luminosity. This is required to calculate the average FRB DM within specific redshift ranges. In the scenario under consideration where the FRBs we associate with nearby galaxies in fact originate within them, the form of dN/dL needs to explain the relative number of nearby FRBs in the CHIME sample. We assume a power-

law form for dN/dL , such that $dN/dL \propto L^{-\gamma}$. For the purposes of this demonstration, we also assume that all FRBs have the same observed widths, so that the detection signal to noise ratio is simply proportional to L/D_L^2 where D_L is the luminosity distance. Various works find $\gamma \sim 1.6 - 1.8$ based on analyses of the FRB samples in hand^{51,52}. We adopt a slightly steeper luminosity function with $\gamma = 2$ for approximate consistency with the apparent nearby-FRB fraction. We confirmed that our results below are largely insensitive to this choice within the $1.5 \leq \gamma \leq 2$ range.

- We then need a model for the extragalactic DM, DM_{EG} , at different redshifts. We write this model as

$$DM_{\text{EG}}(z) = DM_{\text{IGM}}(z) + (1+z)^{-1}DM_{\text{host}} \quad (6)$$

We choose a model for $DM_{\text{IGM}}(z)$ that incorporates the primordial helium fraction and, and has the fraction of cosmic baryons in the IGM as a free parameter f_{IGM} ¹⁷.

- Finally, we calculate the average DM of FRBs within a redshift limit z as

$$\langle DM \rangle(z) = \left[\int_0^z L_0^{1-\gamma}(z') \frac{dV_c}{dz'} dz' \right]^{-1} \int_0^z DM_{\text{EG}}(z') L_0^{1-\gamma}(z') \frac{dV_c}{dz'} dz'. \quad (7)$$

Here, $L_0(z)$ is the limiting luminosity at redshift z ; the specific scale does not affect this calculation.

Extended Data Figure 3 shows the simulated excess DM of the < 40 Mpc sample relative to the sample within different values of the maximum redshift z_{max} . We adopt a fixed $DM_{\text{host}} = 1000 \text{ pc cm}^{-3}$ as an extremal high value, and consider values for f_{IGM} of 0.5 and 0.75. These models struggle to reproduce the observed excess DM of $\sim 200 \pm 100 \text{ pc cm}^{-3}$ for any z_{max} . No

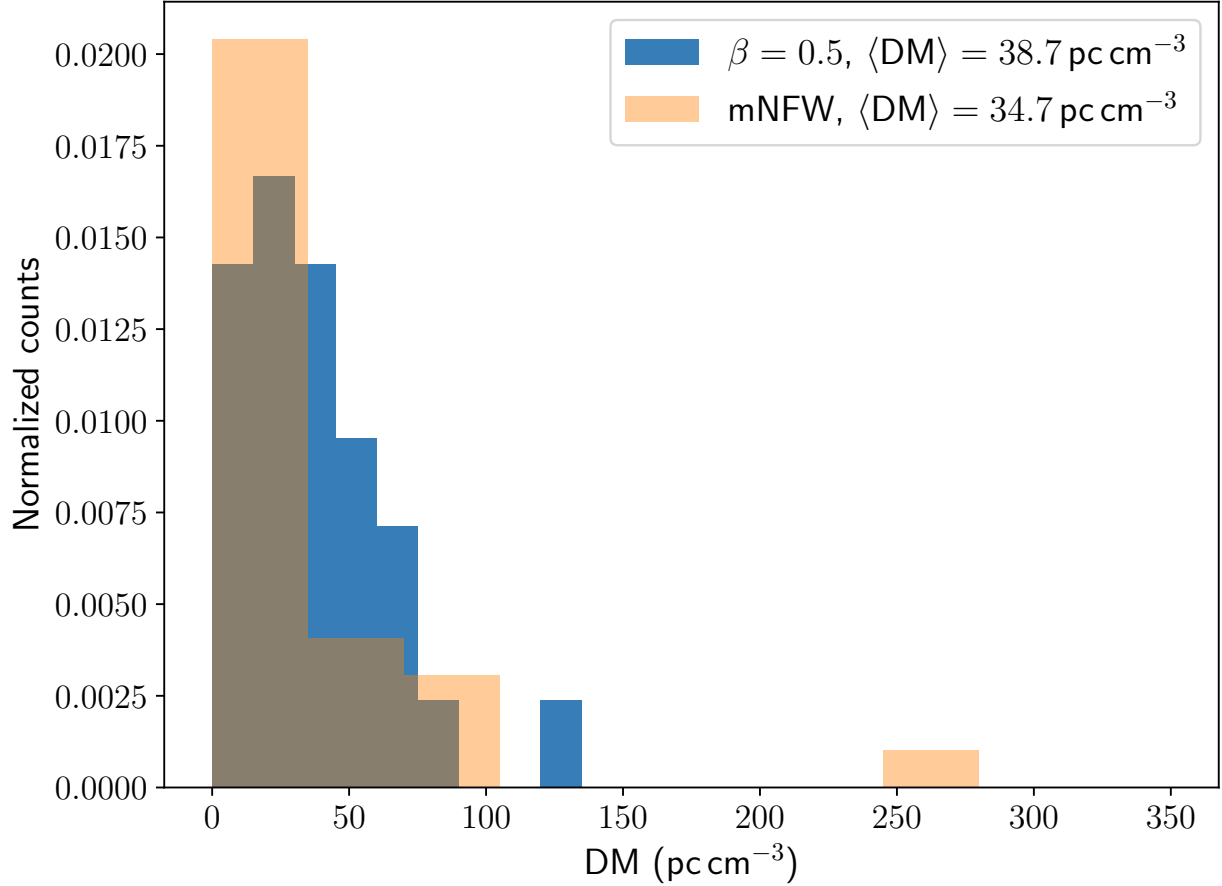
FRB has been observed with $DM_{\text{host}} = 1000 \text{ pc cm}^{-3}$, and it is likely that such FRBs are in fact difficult to observe^{49,50}. Furthermore, in this scenario some FRBs would need to have even more extreme values of $DM_{\text{host}} > 2000 \text{ pc cm}^{-3}$ (Figure 2). The inclusion of some form of stochasticity in our simulations would not change the conclusion that only extreme values of DM_{host} can explain the excess DMs of FRBs associated with nearby galaxy halos. We therefore do not consider this scenario likely.

Data availability statement. The data used in these analyses are all publicly available. The CHIME/FRB Catalog 1 can be found at <https://www.chime-frb.ca/catalog>. The Gravitational Wave Galaxy Catalogue (GWGC) can be downloaded online at <http://vizier.u-strasbg.fr/viz-bin/VizieR?-source=GWGC>.

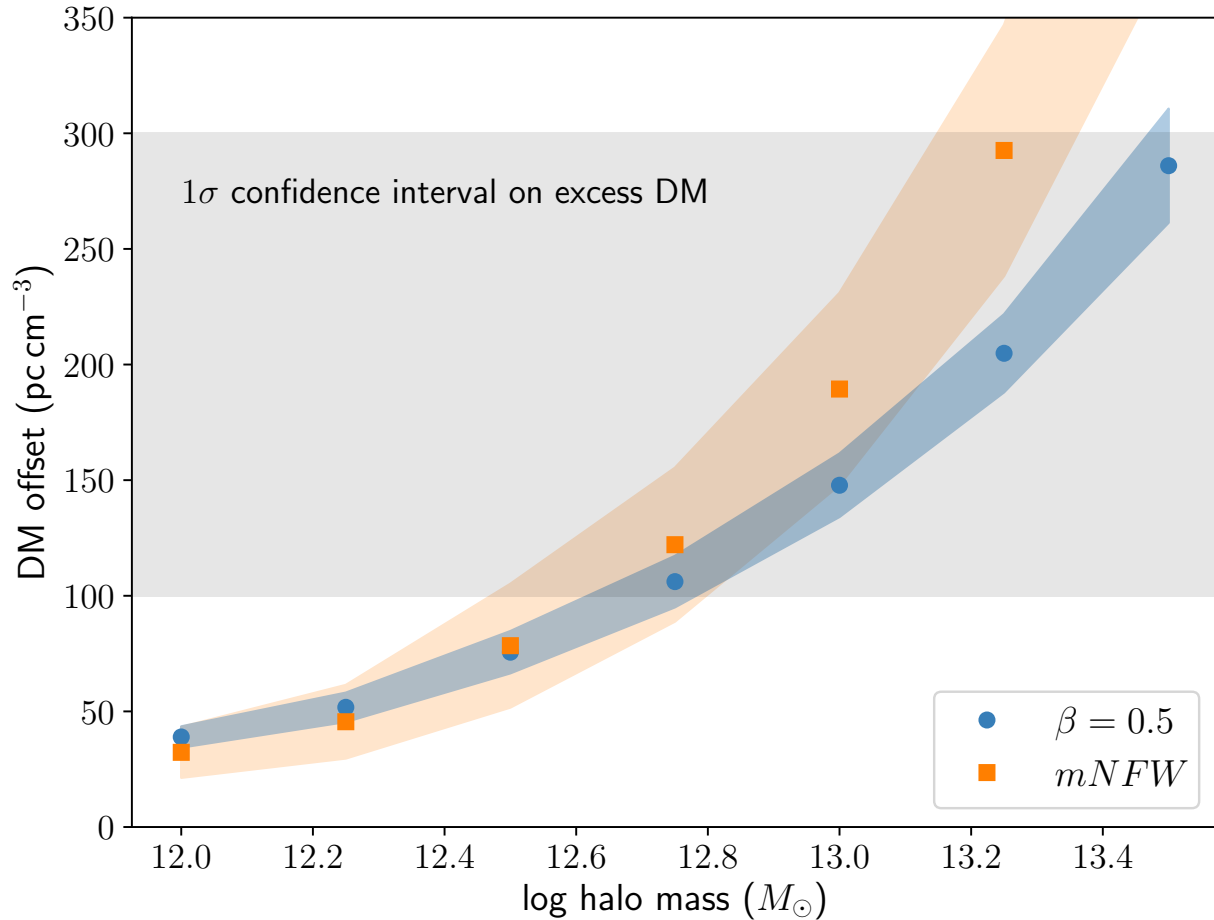
Code availability statement. This research made use of the open-source numpy, scipy, astropy, hmf, NFW, CHIME/FRB’s “cfod” package, and frb (<https://github.com/FRBs/FRB/tree/main/frb>) python packages. All custom code used in our analysis will be made available upon request.

Extended Data Table 1: A table of FRB/foreground galaxy intersections using CHIME/FRB Catalog 1 and GWGC for galaxies within 40 Mpc. We have held b_{\perp} constant at 250 kpc.

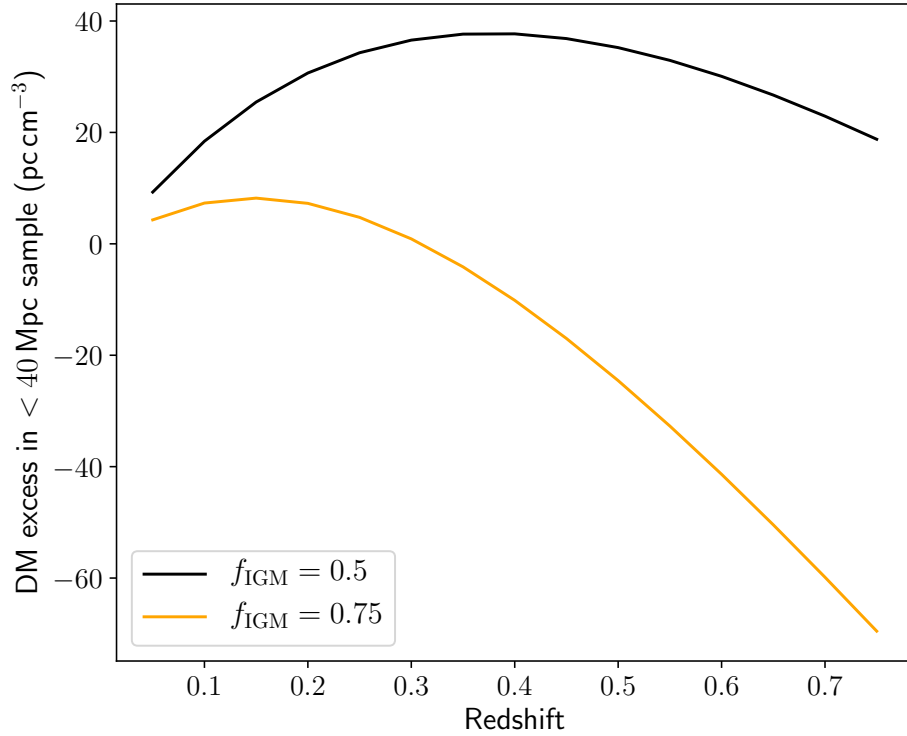
FRB name	Galaxy	Group	Dist (Mpc)	R_{\perp} (kpc)	DM (pc cm⁻³)
FRB20190317E	NGC6615	None	39.1	165	666.6
FRB20190430B	NGC6015	None	15.2	41	2583.0
FRB20190423A	NGC3998	None	14.1	65	211.0
FRB20181214C	NGC3835	None	34.1	92	599.5
FRB20190612A	NGC3034	M81	3.9	71	390.6
FRB20190322B	IC2389	None	33.4	139	530.0
FRB20190701D	NGC2403	M81	3.2	133	877.4
FRB20190130A	NGC0660	M74	9.2	76	1330.1
FRB20190102B	NGC0598	M31	0.8	136	326.1
FRB20190128A	NGC0598	M31	0.8	90	652.5
FRB20190217B	NGC0598	M31	0.8	55	800.4
FRB20190226C	NGC0598	M31	0.8	103	783.3
FRB20190601B	NGC0598	M31	0.8	128	745.9
FRB20190605D	NGC0598	M31	0.8	56	1607.7
FRB20190607A	NGC0598	M31	0.8	109	518.5
FRB20181018A	NGC0224	M31	0.8	164	1008.5
FRB20181101A	NGC0224	M31	0.8	221	1327.8
FRB20190102A	NGC0224	M31	0.8	197	655.6
FRB20190106A	NGC0224	M31	0.8	169	251.2
FRB20190116E	NGC0224	M31	0.8	190	1362.6
FRB20190122B	NGC0224	M31	0.8	139	415.1
FRB20190411C	NGC0224	M31	0.8	275	194.8
FRB20190415B	NGC0224	M31	0.8	185	567.6
FRB20190628C	NGC0224	M31	0.8	101	1649.6



Extended Data Figure 1: Predicted DM excesses for CHIME/FRB galaxy intersections assuming isolated galaxy halos. The histograms show the relative binned counts of DMs accrued by the fiducial sample of 26 FRBs with $b_{\perp} < 250$ kpc. Two models for the radial density distribution of the CGM are shown: a ‘beta’ model with $\beta = 0.5$, and a modified NFW model. Results are shown in blue and orange respectively. The mean DMs of the data shown in each histogram are noted in the figure legend.



Extended Data Figure 2: predicted DM excess for 24 FRBs intersecting halos of different masses. We use a ‘beta’ model with $\beta = 0.5$ and a modified NFW model for the radial density distribution. Results are shown in blue and orange respectively. For each halo mass, 1σ error ranges are shown based on 100 simulations of samples of 24 uniformly distributed FRB intercepts with $b_{\text{perp}} < 250$ kpc. The grey shaded area indicates the 1σ confidence interval corresponding to the measured DM excess of $200 \pm 100 \text{ pc cm}^{-3}$.



Extended Data Figure 3: The excess DM for nearby FRBs relative to populations extending to different redshifts, assuming an unrealistically high local DM. We assign a local $\text{DM}_{\text{host}} = 1000 \text{ pc cm}^{-3}$, and display the difference between the mean DMs of FRBs within 40 Mpc, and FRBs within various redshifts. Three models are considered between the cosmological DM and redshift, parameterized by f_{IGM} .